p-Quinone Dimers: H-Bonding vs Stacked Interaction. Matrix-Isolation Infrared and ab Initio Study

A. M. Plokhotnichenko,[†] E. D. Radchenko,[†] S. G. Stepanian,[†,‡] and L. Adamowicz*[,‡]

Department of Chemistry, University of Arizona, Tucson, Arizona 85721, and Institute for Low-Temperature Physics and Engineering, National Academy of Sciences of Ukraine, 47 Lenin Avenue, Kharkov 310164, Ukraine

Received: June 8, 1999; In Final Form: October 14, 1999

Matrix-isolation IR spectroscopy and ab initio calculations have been used to investigate the structure and the vibrational spectrum of the quinone dimer formed in low-temperature Ar matrices. A specially developed experimental technique was applied to separate the bands of the quinone dimer from the bands of the quinone monomer in the IR spectra. The composition of the matrix samples was precisely controlled with a low-temperature quartz microbalance. As a result, a set of bands assigned to the quinone dimer were identified. Ab initio calculations at the MP2/6-31+G*, MP2/6-31++G**, and DFT/B3LYP/6-31++G** levels of theory have been carried out to determine the relative energies and the vibrational spectra of the two stable configurations of the quinone dimer found in the calculations. These configurations are a planar complex with two weak C−H···O hydrogen bonds and a stacked complex stabilized by the dispersion forces. The MP2 calculations of the interaction energies corrected for the basis set superposition error (BSSE) predict the two dimers to be equally stable. The comparison of the observed IR frequency shifts with the theoretically predicted shifts indicate that only the planar configuration is responsible for all of the experimentally observed dimer bands. Thus, we conclude that the stacked dimer is absent from the matrix. The influence of the matrix environment on the stability shift in favor of the planar dimer is discussed.

1. Introduction

During the past two decades the matrix-isolation IR spectroscopy, coupled with ab initio quantum chemical calculations, has become a powerful investigational tool of structures of molecules and complexes (dimers) with H-bonding interactions. In our recent studies we have also applied this approach to study complexes with weaker H-bonds, such as the C−H···X (X = N, O) interactions, as well as to study stacked dispersion interactions between aromatic rings.[1−3] Investigations of the weak interactions are of great interest because they play an important role in many biological processes. For example, they make an important contribution to the stability of certain structural conformations of nucleic acids.[4] It is well-known that the helical structure of DNA is stabilized not only by H-bonds in the Watson−Crick AT and GC pairs, but also by stacking interactions between the pyrimidine and purine bases along the DNA helical backbone. Recently, Murphy et al.[5] found that stacked heterocycles of DNA serve as an efficient medium for coupling electron donors and acceptors over distances greater than 40 Å. It was also shown that stacking interactions play an important role in the long-distance repair of the DNA radiation-induced damage.[6]

The number of theoretical studies of the stacked interactions between the nucleic acid bases (NAB) has increased significantly during the past few years.[7−14] However, experimental investigations of the NAB weak interactions are still very scarce. We recently reported results of combined matrix-isolation IR and ab initio studies of the competition between C−H···N(O) H-bonding and stacked interactions in the pyrimidine−pyrimidine and pyrimidine−quinone dimers.[1−3] In those investigations, we encountered some difficulties in detecting weakly-bound complexes. These difficulties were related to very weak spectral manifestations of interactions which are significantly weaker than the interactions in complexes with strong H-bonds, such as the N(O)−H···N(O) bonds. When only very weak interactions are present in the complex, the shifts of the IR bands—due to the formation of the dimers with respect to the bands of the monomer—do not typically exceed 10 wavenumbers. For example, these kinds of shifts were observed in the IR spectrum of the pyrimidine dimer. Also, for dimers with very weak interactions, an empirical assignment of the dimer bands to the specific dimer structures is not possible because there is usually a very limited set of IR-active experimental bands which one can use in the assignment. The only way to make positive assignments in such cases is by comparing the experimental IR spectra with the theoretically predicted vibrational frequencies and intensities obtained for all dimer structures, which calculations find to be local minima on the dimer potential energy surface. This approach was used in our previous studies of the pyrimidine−pyrimidine and pyrimidine−quinone dimers.[1−3] As a result of those works, we established some interesting relations between the structural features of the weakly bonded dimers and their IR spectra. For example, we determined that the stacked interaction should cause a stronger shift of the bands corresponding to the C−H stretching vibrations than the C−H···N(O) H-bond interaction.

Another difficulty in IR studies of weak complexes is related to the low intensities of the dimer bands in the matrix spectra. It is well-known that a strong H-bond leads to a significant

* Corresponding author. E-mail: ludwik@u.arizona.edu. Fax: (520) 621-8407.
[†] University of Arizona.
[‡] National Academy of Sciences of Ukraine.

10.1021/jp991869a CCC: $18.00
Published on Web 11/19/1999

increase of the intensities of the IR bands corresponding to vibrations of the atoms and the group of atoms directly involved in the H-bond interaction. This phenomenon enables identification of the IR dimer bands and separating them from the monomer bands. But the intensity increase is much smaller for very weakly-bonded dimers. The small intensity of the dimer bands requires registration of the IR matrix-isolation spectra for samples with the highest possible concentration of the dimers relative to the concentration of the monomers. In the previous studies on homodimers[3,15] and heterodimers,[1] we determined how to achieve the optimal matrix concentration of the dimers, enabling their spectral detection. The procedure we developed, which was based on the use of the low-temperature quartz microbalance described previously,[17] allows for precise monitoring of the concentrations of the matrix-deposited substances.

In our previous works on weakly-bonded complexes, we analyzed the structures of pyrimidine−pyrimidine homodimers[3] and pyrimidine−quinone heterodimers[1] based on matrix-isolation IR spectra and on the results of ab initio calculations. For the pyrimidine−quinone system we assigned the observed dimer IR bands to the planar dimer stabilized by the C−H···O and C−H···N H-bonds, based on a very good agreement between the observed bands and the vibrational frequencies predicted for this dimer by the calculations. However, for the pyrimidine−pyrimidine system, the agreement between the observed and calculated spectra was not so perfect. We now believe that this was probably due to a larger number of possible different pyrimidine−pyrimidine dimer structures which was present in the matrix. The calculations supported this conclusion. We found as many as four, almost isoenergetic, dimer structures—three planar and one stacked in the calculations. If all these predicted dimers are presented in the matrix, the assignment of the IR bands becomes difficult and the harmonic frequencies calculated at a lower level of theory (e.g., at the HF level) may not be sufficiently accurate to distinguish and assign the spectral features to different dimer structures.

In this work, we present results of the experimental and theoretical investigations of the quinone homodimer. Quinone can form only weak C−H···O H-bonds which have a similar strength as the stacking interaction, and both H-bonded and stacked dimers of this system may be formed in the matrices. Moreover, due to its high symmetry (D_{2h}), quinone is a very suitable model for such study because it can form only a very limited number of different dimers. The main goal of this study is to determine whether the matrix-isolated quinone dimers are H-bonded or/and stacked.

The matrix-isolation IR spectra of the quinone dimer spectra were obtained using a similar procedure as applied before in studies of pyrimidine−pyrimidine and pyrimidine−quinone dimers. The interaction energies in the dimers were calculated using the second-order Møller−Plesset perturbation theory (MP2) method, and the density functional theory (DFT) method was used in the harmonic frequency calculations.

2. Experimental Method

The matrix samples were prepared by simultaneous deposition of the substance and the matrix gas (Ar) onto a cooled CsI substrate. The substrate temperature was maintained at 16−18 K during the matrix deposition to obtain samples with optimal scattering. To prevent matrix overheating in the spectrometer beam, the samples were cooled to 12 K for spectra recording. The matrix gas was 99.99% Ar. The concentrations of the substances were controlled using a low-temperature quartz microbalance. The flow stability of the components was achieved with a stable gas pressure over the solid phase at fixed temperatures of 30 °C for quinone and 77 K for Ar. The densities of the substance flows were controlled with fine control valves.[16] To avoid condensation of quinone, the control valve and the connecting tubes were heated to 70 °C. The fill-up helium cryostat used for the matrix-isolation IR spectroscopy in the present work was described elsewhere.[17] The updated SPECORD IR 75 grating spectrometer was sealed and blown through with dry nitrogen during the experiment to exclude the influence of atmospheric the H_2O and CO_2 vapor. The IR spectra were registered in the range of 4000−400 cm^{-1}. The resolution of 3 cm^{-1} was achieved near 3000 cm^{-1}, and the resolution of 1 cm^{-1} was achieved in the spectral range of 2500−400 cm^{-1}. The absolute amounts of the deposited substances were determined from the flow densities and the duration of the deposition. We should mention that the integrated absorption coefficients may be considerably underestimated for some bands, since half-widths of the bands in the matrix IR spectra are much smaller than the spread function width of the spectrometer. The spectra of quinone were scaled by assuming the surface quinone density of 3.0×10^{-5} g/cm^2 in the samples.

The IR spectrum of the quinone monomer was registered for samples with the substance-to-matrix ratio of 1:1000. The low-temperature quartz microbalance[17] was used to measure the concentrations of the gaseous flows of quinone and the Ar gas. At the concentration of 1:1000, more than 95% of all quinone molecules were found in the monomer form. To register the IR spectra of the quinone dimer, we deposited samples with the matrix ratio of 1:250. Earlier,[1,15] we demonstrated that this matrix ratio is optimal for investigating dimers. When the substance−matrix concentration increases from 1:1000 to 1:250, the concentration of the dimers increases to 16% when measured immediately after matrix deposition, and to 25% after matrix annealing. A further increase of the substance−matrix concentration results in a decrease of the dimer concentration due to a preferential formation of larger disordered complexes. For example, when the concentration increases from 1:250 to 1:125, the percentage of the larger complexes increases from ≈5% to ≈37%.

3. Computational Details

The geometries of the quinone dimers were fully optimized at the MP2 level of theory[18,19] with the 6-31-type Gaussian basis set augmented with the standard diffuse and polarization functions on the heavy atoms (the 6-31+G* basis). The calculations converged to two equilibrium structures of the quinone dimer. They are the *planar* dimer stabilized by the C−H···O H-bonds and the stacked dimer stabilized by the dispersion interaction. The equilibrium dimer structures are shown in Figure 1. The interaction energies in the dimers were calculated with accounting for the basis set superposition error (BSSE) using the counterpoise method of Boys and Bernardi.[20] This involves a single calculation for the dimer and two calculations for the monomers with the basis set of the dimer performed at the monomer equilibrium geometries.

The necessity of having to use the harmonic approximation in the frequency calculations for the quinone dimers, whose results were needed to assist in the analysis of the experimental IR spectra, created a dilemma. The limitations of the computer resources available to us precluded application of the MP2 method in determining the harmonic frequencies. On the other hand, as we demonstrated earlier, the HF and DFT methods are unable to describe the dispersion interaction stabilizing two aromatic rings in a stacked conformation, and render it

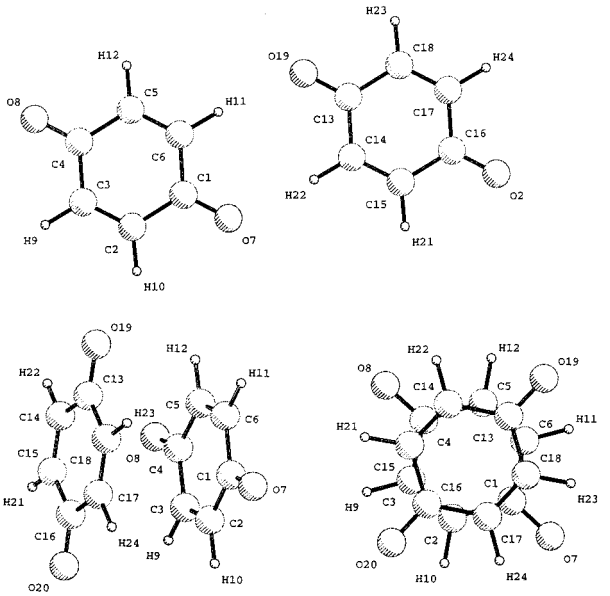

Figure 1. Equilibrium geometries of the planar (top) and stacked (bottom, two views) quinone dimers obtained at the MP2/6-31+G* level of theory. (The geometries are available from the corresponding author.)

unstable.[1−3] All attempts to find the stacked equilibrium structure for the quinone dimer at these levels of theory failed. In this situation we were forced to use an alternative method to calculate the IR frequencies for the quinone dimers and the procedure is described in the next paragraph.

The geometries of the planar and stacked dimers were first fully optimized at the MP2/6-31+G* level of theory. The intramolecular coordinates for each dimer were then reoptimized, using the DFT/B3LYP method[21−23] with the 6-31++G** basis set while the six intermolecular parameters (the internal coordinates of the dimers describing the relative orientation of the two monomers) were frozen. For the structures obtained in these calculations, DFT/B3LYP/6-31++G** harmonic frequencies were calculated. The obtained DFT frequencies corresponding to the intermolecular vibrational modes are suspect since the intermolecular parameters were not optimal at the DFT level. In fact, this method produced an imaginary frequency for the lowest vibrational mode for each dimer. However, this did not produce any practical difficulties for our study since the experimental procedure did not probe the low-frequency region. The harmonic frequencies of the quinone monomer were also calculated at the DFT/B3LYP/6-31++G** level and compared with the DFT intramolecular frequencies obtained for the dimers. Additionally, MP2/6-31++G** calculations for the dimers were carried out using geometries optimized at the MP2/6-31+G* level. All calculations presented in this work were performed using the GAUSSIAN 94 software package.[24]

4. Results and Discussion

4.1. Experimental Matrix-Isolation IR Spectra of the Quinone Monomer and Quinone Dimers. The fingerprint region of the quinone IR spectrum obtained for the sample with matrix ratio of 1:1000 is presented in Figure 2. The quinone monomer vibrational frequencies and IR intensities are collected in Table 1. The DFT/B3LYP/6-31++G** harmonic frequencies, intensities, and potential energy distributions (PED) of the quinone monomer are also presented in Table 2. The calculated frequencies were scaled with the scaling factor of 0.95 for the C−H stretches and with the scaling factor of 0.98 for all other

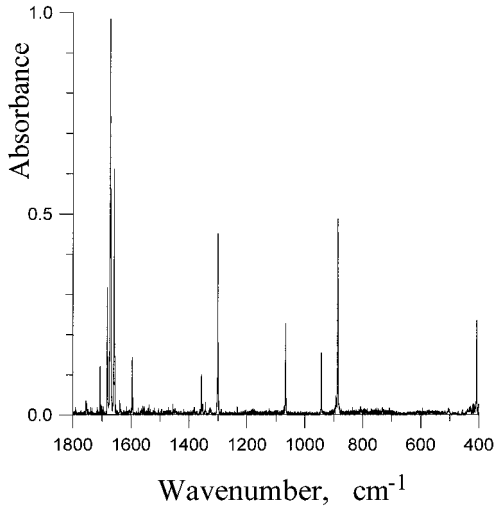

Figure 2. Matrix IR spectrum of quinone (1800−400 cm^{-1}) registered for the sample with the matrix ratio of 1:1000 (quinone:Ar) at 12 K.

TABLE 1: Experimental and Selected Predicted Frequencies (ω, cm^{-1}) and Intensities of the Quinone Monomer and the Quinone Dimers

observed[a]			calculated[b,c]			
monomer		dimer	monomer		planar	stacked
ω	I	shift[d]	ω	I	dimer shift[d]	dimer shift[c]
1755	3.5	0				
1707	5.3	0				
1682	25	0				
1672	70	0				
1670	40	(−9)[e]	1700	447.1	−7	−2
1659	52	(+2)[e]				
1640	2.9	0				
1596	9	?[f]				
1357	4.7	0				
1353	2	0				
1301	3	+2.5	1295	78.9	+4	−2
1066	17	+4.5	1065	44.7	+7	0
942	9	0				
886	50	+6.5	883	83.0	+7	0
503	2.9	0				
407	18	+3	404	25.2	+4	0

[a] Spectra observed for quinone isolated in Ar matrix at 12 K. Matrix ratio of 1:1000 for the quinone monomer IR spectrum and 1:250 for the quinone dimer IR spectrum. [b] Calculated at the DFT/B3LYP/6-31++G** level for the quinone monomer geometry fully optimized at the same level and for the dimer geometries with intramolecular parameters optimized at the DFT/B3LYP/6-31++G** level and intermolecular parameters optimized at the MP2/6-31+G* level. [c] Selected calculated frequencies corresponding to the observed ones. The whole calculated spectra of the quinone monomer and dimers are given in Tables 2 and 3. [d] Shifts in cm^{-1} with respect to the corresponding monomer bands. [e] New band appeared in the quinone dimer spectrum at 1661^{-1}. It may originate from 1670 or 1659 cm^{-1} bands of the monomer. See discussion in the text. [f] The monomer band is weak; we suspect the presence of shifted band of the dimer in the spectrum, but due to the low intensity we cannot define its accurate location.

vibrations. The comparison of the observed and calculated data for the quinone monomer reveals a favorable agreement for all vibrations except the C═O stretching. While the calculations predict only one band corresponding to the IR-active asymmetric vibration of the C═O bonds, a set of split bands in the C═O stretching region of the experimental spectrum is observed. This phenomenon is typical of the C═O stretches and is due to the Fermi resonance and the site splitting. This splitting hampers a

TABLE 2: Harmonic Frequencies (ω, cm^{-1}) and Intensities (I, km mol^{-1}) Calculated at the DFT/B3LYP/6-31++G Level for the Quinone Monomer**

ω^2	I	assignment[b]
3054	0	C3H9 str [25], C2H10 str [25], C6H11 str [25], C5−H12 str [25]
3052	4.5	C3H9 str [25], C2H10 str [25], C6H11 str [25], C5H12 str[25]
3037	0	C3H9 str [25], C2H10 str [25], C6H11 str [25], C5H12 str[25]
3036	1.6	C3H9 str [25], C2H10 str [25], C6H11 str [25], C5H12 str[25]
1702	0	C1O7 str [33], C4O8 str [30], C5C6 str [10]
1700	447.1	C4O8 str [46], C1O7 str [43]
1646	0.	C5C6 str [34], C2C3 str [27], C1O7 str [15], C4O8 str [15]
1615	16.8	C2C3 str [46], C5C6 str [46]
1371	0	C2C3C4 bend [18], C3C4 str [16], C2C3H9 bend [16], C5C6H11 bend [16], C6C5H12 bend [16], C1C2C3 bend [15], C1C2 str [12], C4C5C6 bend [11], C1C2H10 bend [11]
1358	4.8	C2C3H9 bend [23], C5C6H11 bend [23], C6C5H12 bend [23], C1C2H10 bend [18]
1295	78.9	C1C2 str [23], C4C5 str [23], C2C3C4 bend [12]
1213	0	C4C5C6 bend [20], C1C2 str [17], C3C4 str [17], C1C2H10 bend [13]
1145	0	C2C3H9 bend [22], C5C6H11 bend [22], C6C5H12 bend [22], C1C2H10 bend [21]
1065	44.7	C2C3H9 bend [17], C5C6H11 bend [17], C6C5H12 bend [17], C1C2H10 bend [14]
990	0	C1C2C3C4 tor [23], C1C2C3H9 tor [22], C3C4C5C6 tor [21], C6C1C2H10 tor [21], C4C5C6H11 tor [21], C1C6C5H12 tor [21]
989	0	C6C1C2H10 tor [24], C4C5C6H11 tor [21], C1C6C5H12 tor [21], C1C2C3H9 tor [20]
929	19.4	C4C5C6 bend [66], C2C3C4 bend [−45], C3C4C5 bend [25], C1C2C3 bend [16]
883	83.0	C2C3C4C5 tor [41], C1C2C3H9 tor [18], C4C5C6H11 tor [18], C1C6C5H12 tor [18]
766	0	C1C2C3C4 tor [76], C3C4C5C6 tor [41], C2C3C4C5 tor [−36]
759	0	C3C4 str [45], C4C5 str [35], C3C4C5 bend [26]
740	0.5	C3C4C5 bend [70], C2C3C4 bend [−23], C1C2C3 bend [20], C1C2 str [13], C4C5 str [13]
740	0	C1C2C3H9 tor [25], C6C1C2H10 tor [25], C4C5C6H11 tor [25], C1C6C5H12 tor [25]
589	0	C2C3C4 bend [27], C3C4 str [18], C2C1O7 bend [17], C3C4O8 bend [17]
504	4	C2C3C4C5 tor [39], C6C1C2H10 tor [15], C3C2C1O7 tor [12], C2C3C4O8 tor [12]
447	0	C4C5C6 bend [29], C2C1O7 bend [24], C3C4O8 bend [24], C1C2C3 bend [22]
445	0	C1C2C3 bend [36], C3C4C5 bend [30], C2C3C4 bend [29]
404	25.2	C2C1O7 bend [36], C3C4O8 bend [36], C2C3C4 bend [11]
330	0	C2C3C4C5 tor [50], C3C4C5C6 tor [45]
219	0	C3C2C1O7 tor [45], C2C3C4O8 tor [45], C3C4C5C6 tor [31]
94	15.3	C2C3C4C5 tor [51], C3C2C1O7 tor [32], C2C3C4O8 tor [32]

[a] Frequencies are scaled with the following scaling factors: 0.95 for the C−H stretching vibrations and 0.98 for all other vibrations. [b] Potential energy distributions are given in square brackets. Only contributions ≥ 10% are listed. Abbreviations: str, stretching; bend, bending; tor, torsion.

direct comparison of the observed and calculated data. Overall, the largest difference between the calculated and observed frequencies is 19 cm^{-1} and the mean difference is only 6 cm^{-1}. These values demonstrate that the DFT method with the B3LYP functional performs very well in predicting the quinone vibrational features.

An increase of the quinone concentration in the matrix from 1:1000 to 1:250 (quinone:Ar) leads to an appearance in the IR spectra of an additional set of bands which are attributed to the quinone dimers formed in the matrix at this concentration. A total of five new bands were registered in the IR spectra. The values of the frequency shifts of the bands (with respect to the corresponding monomer bands) are given in Table 1. Some spectral regions, where the dimer bands appeared, are presented in Figure 3. It is notable that the half-widths of the dimer bands only slightly exceed the half-widths of the monomer bands. This minimal broadening indicates that the quinone dimers have well-defined structures. Four observed dimer bands are up-shifted with respect to the corresponding monomer bands. These dimer bands are attributed to the ring stretching vibration (1303 cm^{-1}), the C−H bending vibration (1070.5 cm^{-1}), the C−H out-of-plane vibration (892.5 cm^{-1}) and the C═O bending vibration (410 cm^{-1}). As seen from Table 1 and Figure 3, only one quinone dimer band was observed in the C═O stretching vibration region at 1661 cm^{-1}. As mentioned previously, the band of the C═O stretching vibration of the monomer is split and this dimer band can be correlated to the monomer bands at either 1670 or 1659 cm^{-1} with corresponding shift values of −9 or +2 cm^{-1}, respectively. One realizes that we have observed only a few dimer bands in the IR spectrum. This result

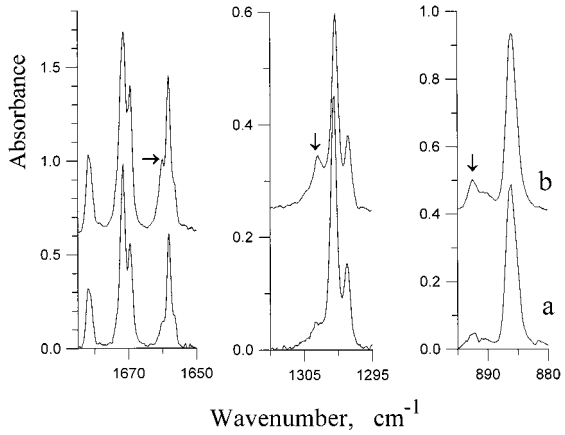

Figure 3. Fragments of the IR spectra of quinone (T = 12 K) for the matrix ratio of 1:1000 (a) and 1:250 (b). Arrows indicate the bands attributed to the quinone dimers.

is in line with the total number of the observed bands for the quinone monomer, which is also small due to its high symmetry. In fact, as seen in Table 1, the shifted dimer bands were registered for all the intensive bands of the monomer.

4.2. Structure of the Quinone Dimers. To determine the structure of the quinone dimers formed in the Ar matrix, we compared the experimental dimer frequency shifts (see Table 1) with the frequency shifts predicted in the DFT/B3LYP/6-31++G** calculations for the two dimers, planar and stacked (see Figure 1). The calculated frequencies of the dimers are presented in Table 3.

TABLE 3: Harmonic IR Frequencies (ω, cm^{-1}) and Intensities (I, km mol^{-1}) Calculated at the DFT/B3LYP/6-31++G Level of Theory for the Quinone Dimers**

monomer		planar dimer				stacked dimer			
ω	I	ω	I	ω	I	ω	I	ω	I
3054	0.0	3053	0.6	3053	6.2	3056	0.0	3056	0.0
3052	4.5	3048	11.4	3047	6.7	3054	0.2	3053	0.4
3037	0.0	3036	1.4	3036	1.3	3040	0.1	3040	0.2
3036	1.6	3029	80.3	3024	56.8	3038	0.3	3038	0.3
1702	0.2	1702	51.3	1701	0.1	1703	6.2	1699	134.6
1700	447.1	1693	1024.8	1689	0.3	1698	403.5	1698	264.9
1646	0.0	1643	8.4	1643	0.0	1643	0.4	1642	2.8
1615	16.8	1614	0.7	1614	43.6	1612	16.3	1612	15.8
1371	0.0	1379	0.2	1375	13.9	1371	0.0	1370	0.0
1358	4.8	1363	0.0	1362	10.1	1358	4.7	1358	4.6
1295	78.9	1302	0.1	1299	167.2	1294	42.5	1293	41.4
1213	0.0	1219	0.0	1217	0.5	1212	0.0	1211	0.0
1145	0.0	1156	0.0	1154	0.2	1146	0.0	1146	0.0
1065	44.7	1073	8.6	1072	68.6	1065	27.3	1065	26.8
990	0.0	1011	0.8	1004	0.0	997	0.3	995	0.1
989	0.0	989	0.0	989	0.0	994	0.2	992	0.0
929	19.4	930	55.9	930	12.0	929	17.6	929	17.5
883	83.0	890	156.7	887	0.1	886	1.0	883	199.4
766	0.0	762	0.0	761	1.7	772	0.2	769	0.2
759	0.0	756	0.0	753	1.3	760	0.1	759	0.0
740	0.5	750	0.1	747	0.9	746	2.5	744	4.2
740	0.0	744	3.8	743	0.0	741	0.4	740	0.5
589	0.0	592	0.0	590	0.6	590	0.0	588	0.0
504	4.3	514	0.0	509	6.3	507	3.5	505	0.3
447	0.0	451	4.3	449	0.0	447	0.0	446	0.0
445	0.0	448	1.5	445	0.0	445	0.2	445	0.2
404	25.2	408	64.6	406	0.0	404	19.3	404	19.3
330	0.0	330	0.0	329	0.0	333	0.3	324	0.2
219	0.0	213	0.1	207	0.0	230	0.2	226	0.3
94	15.3	98	27.2	89	0.1	104	29.2	101	6.5
				73	0.0			83	0.4
				48	0.0			66	1.0
				44	0.0			55	0.2
				41	1.3			43	0.1
				27	0.4			39	0.1
				12	0.0			12	0.0

[a] Frequencies are scaled with the following scaling factors: 0.95 for the C−H stretching vibrations and 0.98 for all other vibrations.

For the four bands observed at 1301, 1066, 886, and 407 cm^{-1} for the quinone monomers, the observed shifts of the corresponding dimer bands are +2.5, +4.5, +6.5, and +3 cm^{-1}. As seen from Table 1 for these frequencies, the calculations predict different shifts for the planar and stacked dimers. While the shifts calculated for the planar dimer (+4, +7, +7, and +4 cm^{-1}, respectively) clearly agree very well with the experimental shifts, the shifts for the stacked dimer, which are −2, 0, 0, and 0 cm^{-1}, do not agree. Particularly, the lack of a down-shifted band (by about −2 cm^{-1}) from the 1301 cm^{-1} monomer band in the experimental spectrum is an indication that the stacked dimer is absent from the matrix. Therefore, we concluded that the planar quinone dimer is responsible for the experimentally observed shifts.

As stated, there was a quinone dimer band registered in the C═O vibration region at 1661 cm^{-1}. It may have originated from the monomer 1670 cm^{-1} band shifted by −7 cm^{-1} or from the monomer 1659 cm^{-1} band shifted by +2 cm^{-1}. For this band, calculations predict shifts of −9 cm^{-1} for the planar dimer and −2 cm^{-1} for the stacked dimer. The shift predicted for the stacked dimer matches none of the experimental shifts. At the same time, the shift predicted for the planar dimer agrees well with one of the two experimental shifts. This confirms the conclusion that the planar quinone dimer is the only form of the dimer present in the matrix.

The potential energy distribution analysis for the shifted bands (Table 2) demonstrates that most of them are assigned to the C═O stretching and bending vibrations and to the C−H bending and out-of-plane vibrations, i.e., to vibrations of those quinone fragments which are directly involved in the C−H···O H-bonds in the planar dimer. The calculations also predict lower frequency shifts for the C−H stretching vibrations for this dimer, but these vibrations are not expected to be observed in the IR spectrum of quinone due to their low predicted intensities. The observed lower frequency shifts for the stretching vibrations and higher frequency shifts for the bending and out-of-plane vibrations are very similar to the spectral manifestation of a strong H-bond. At the same time, there are some notable differences. The shifts caused by weak H-bonds do not exceed 10 cm^{-1}, in contrast to the shifts of up to a few hundreds of wavenumbers for the X−H stretches and up to a few tens of wavenumbers for other vibrations in the case of a strong H-bond. Weak H-bonds also cause little intensity change of the IR bands. For all the dimer bands observed in the matrix, the calculations predict intensity increase by approximately a factor of 2 (see Table 3). Even so, we should not forget that the dimer concentration in the matrix is 2 times smaller than the concentration of the quinone monomer and, in effect, no significant intensity change should be observed.

4.3. Relative Stabilities of the Quinone Dimers. The MP2/6-31++G** energies of the planar and stacked dimers calculated with the geometries optimized at the MP2/6-31+G* level are presented in Table 4. When the BSSE and ZPVE corrections are not accounted for, the stacked dimer is more stable than the planar dimer. The relative energy of the planar dimer with respect to the stacked dimer is 17.2 kJ mol^{-1} at the MP2/6-

TABLE 4: MP2/6-31+G* and MP2/6-31++G//MP2/6-31+G* Energies (au), Interaction Energies (IE, kJ mol^{-1}), and Zero-Point Vibration Energies (ZPVE, au) for the Quinone Planar and Stacked Dimers, and BSSE- and ZPVE-Corrected Interaction Energies[a]**

	MP2/6-31+G*		MP2/6-31++G**// MP2/6-31+G*	
	planar dimer	stacked dimer	planar dimer	stacked dimer
energy	−760.713125	−760.719683	−760.774270	−760.780557
IE	−25.4	−42.6	−26.4	−42.9
ZPVE[b]	0.170468	0.170563	0.170468	0.170563
ZPVE correction	0.000776	0.000871	0.000776	0.000871
BSSE correction[c]	0.002835	0.009126	0.003036	0.009271
IE (BSSE corrected)	−18.0	−18.7	−18.4	−18.6
IE (BSSE and ZPVE corrected)	−15.9	−16.4	−16.4	−16.3

[a] All the energies except ZPVE's were obtained for the MP2/6-31+G* dimer geometries. [b] Harmonic frequencies were calculated at the DFT/B3LYP/6-31++G** level for the dimer geometries with intramolecular parameters optimized at the DFT/B3LYP/6-31++G** level and intermolecular parameters optimized at the MP2/6-31+G* level. [c] Energy difference calculated for the equilibrium monomer geometries in the monomer and dimer basis sets.

31+G* level and 16.5 kJ mol^{-1} at the MP2/6-31++G** level. Accounting for the BSSE and ZPVE corrections almost nullifies the difference in the interaction energy of the two dimers. This is due to the MP2/6-31+G* BSSE's being significantly different for the planar and stacked dimers (7.4 and 24.0 kJ mol^{-1}, respectively). Similar results were obtained previously for the planar and stacked pyrimidine homodimers[3] and quinone−pyrimidine heterodimers.[1] The BSSE for the stacked dimer is larger than for the planar dimer because the atoms of the two monomers in the former configuration are closer together, leading to a more effective sharing of the basis functions.

The gradient optimization implemented in the GAUSSIAN 94 program,[24] which we used to determine the equilibrium dimer structures, does not include the BSSE correction. This correction for the stacked dimer is almost equal to its total interaction energy and may affect both the calculated equilibrium structure and the interaction energy of the dimer. To investigate this effect, we carried out additional MP2/6-31+G* calculations of the BSSE-corrected interaction energies for the stacked dimer for different separations between quinone molecules in the proximity of the optimal separation (determined in the gradient optimization) to find the point corresponding to the energy minimum of the interation energy (i.e., its most negative value). The minimal BSSE-corrected interaction energy was found to be −20.4 kJ mol^{-1}. This value is 1.7 kJ mol^{-1} lower than the BSSE-corrected interaction energy obtained for the equilibrium configuration determined in the gradient optimization. The minimal interaction energy corresponds to the dimer configuration with the intermolecular distance of 3.49 Å, which is slightly larger than the value 3.28 Å obtained in the gradient optimization. The elongation of the intermolecular distance in the equilibrium stacked configuration, when the BSSE correction is accounted for in the calculation, is an expected result because the BSSE artificially lowers the total energy of the dimer more for shorter separations than for larger ones, resulting in the BSSE-uncorrected geometry optimization to underestimate the intermolecular distance. The decrease of the interaction energy by 1.7 kJ mol^{-1} is insignificant and results in virtually no change in the predicted relative stability of the planar and stacked quinone dimers.

As mentioned, the MP2 interaction energies for the planar and stacked dimers with accounting for the BSSE and ZPVE corrections are very close. This result seems to contradict the conclusion derived from the analysis of the experimental IR spectra which indicated that only the planar dimer is present in the matrix. However, one needs to take into consideration that the calculated results correspond to isolated quinone dimers, while in matrices the dimers interact with the matrix environment. This interaction is less important for strongly H-bonded complexes where the H-bond interaction energies are a few times higher than the interaction of the complexes with the matrix material. The interaction energies in the quinone dimers in the range of −20 kJ mol^{-1} are comparable to the interaction energies of the dimers with the matrix, and in evaluating the relative stability of the dimers, their interactions with the matrix have to be accounted for.

To account for the matrix influence on the formation of the quinone dimer, one needs to determine the interaction energies of the quinone monomer and dimers with the matrix material. This involves calculations of the interaction energies of the planar and stacked dimers, as well as the quinone monomer, with at least all of the argon atoms situated in the first coordination spheres of these systems. Naturally, calculations of these interaction energies at the level used in the isolated dimer calculations were not possible because the first coordination spheres consist of as many as 35−40 Ar atoms. Therefore, the interactions were estimated using a less sophisticated approach. The estimation was based on the dimer interaction energies calculated in this work, on the Ar−Ar interaction energy derived from the experiment,[25] and on the interaction energies which we additionally calculated for complexes of a single argon atom and the quinone monomer. These latter calculations were carried out at the MP2/6-31+G* level of theory and included the planar quinone−Ar dimers with the Ar atom interacting with the terminal hydrogen and/or oxygen atoms in quinone, and the stacked quinone−Ar conformer with the Ar atom interacting with the quinone π-system. The average BSSE-corrected interaction energies obtained in the calculations were as follows: $\approx$−6 kJ mol^{-1} for the planar quinone−Ar dimers (we denote this quantity as $IE_{ArQ.planar}$) and $\approx$ −8 kJ mol^{-1} for the stacked quinone−Ar dimer (we denote this quantity as $IE_{ArQ.stacked}$).

To evaluate the interaction energies of the quinone monomer and the quinone dimers with the first coordination spheres in the matrix, information about the stuctures of the spheres was required. The molar volume of quinone (calculated using quinone molecular weight and density) is 81.8 cm^3 mol^{-1} and it is almost 4 times larger than the molecular volume of argon (22.6 cm^3 mol^{-1}). Assuming that the quinone molecule is planar and its width is almost equal to the diameter of the Ar atom, it is reasonable to assume that the quinone molecule in the matrix occupies a cavity formed by removing four Ar atoms from one of the planes of the Ar closed-packed crystal (see Figure 4). Furthermore, we assume that the planar quinone dimer occupies a cavity which is twice the size of the cavity for the monomer. The following perturbations and the related energy contributions accompany the formation of the planar quinone dimer in the matrix from two matrix-deposited monomer molecules.

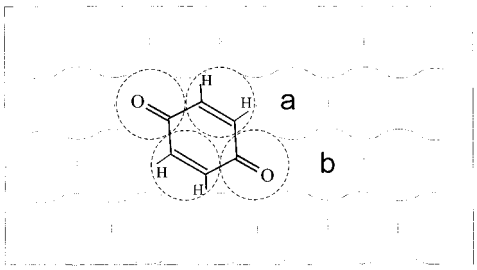

Figure 4. Positioning of the quinone molecule in the closed-packed Ar crystal.

1. In order for the two monomer molecules to form C−H···O H-bonds between each other, two argon atoms must be removed from the first coordination sphere of each. These argon atoms are indicated as a and b in Figure 4. Separating the argon atoms from the two quinone monomers results in the net energy contribution equal to 4 times the average interaction energy of a single argon atom with the quinone monomer in a planar conformation: i.e., $-4 \cdot IE_{ArQ.planar}$.

2. The interactions of the two quinone molecules with the four argon atoms, which are removed to enable formation of the dimer, are replaced for these atoms by interactions with other argon atoms when the four atoms are moved to the bulk. As one can see from Figure 4, replacing the quinone molecule in the cavity by argon atoms results in formation of two Ar−Ar interactions for atom a and one Ar−Ar interaction for atom b. Therefore, for two pairs of argon atoms separated from the two quinone monomers, the total energy contribution due to the new Ar−Ar interactions is equal to 6 times the single Ar−Ar interaction energy: i.e., $6 \cdot IE_{ArAr}$. This energy can be estimated from the sublimation heat of argon at low temperature which is equal to 8.1 kJ mol^{-1}.[25] Since in the closed-packed crystal each argon atom interacts with six other argon atoms, the single argon−argon interaction energy, IE_{ArAr}, can be estimated as -1.3 kJ mol^{-1}.

3. When a planar quinone dimer is formed, the energy contribution is equal to the quinone−quinone interaction energy calculated for the planar conformer, which we denote as $IE_{QQ.planar}$.

4. Thus, the total energy contribution due to formation of the planar dimer, ΔE_{planar}, can be estimated as

$$\Delta E_{planar} = IE_{QQ.planar} - 4 \cdot IE_{ArQ.planar} + 6 \cdot IE_{ArAr} \approx 0 \text{ kJ mol}^{-1}$$

A similar analysis can be performed for the stacked quinone dimer and the respective energy contributions can be estimated as follows:

1. In order to enable a vertical contact of two quinone molecules and their stacked π interaction, four argon atoms need to be removed from one side of each of the molecules. This results in eight Ar−quinone removed interactions, whose combined energy contribution is equal to $-8 \cdot IE_{ArQ.stacked}$.

2. Based on a similar analysis as for the planar dimer, one can determine that the removed and transferred to bulk eight argon atoms will form 18 new Ar−Ar interactions. The energy contribution due to these interactions is equal to $18 \cdot IE_{ArAr}$.

3. When a stacked quinone dimer is formed, the energy is equal to $IE_{QQ.stacked}$.

4. Thus, the total energy contribution due to formation of the stacked quinone dimer, $\Delta E_{stacked}$, can be esimated as

$$\Delta E_{stacked} = IE_{QQ.stacked} - 4 \cdot IE_{ArQ.stacked} + 6 \cdot IE_{ArAr} \approx +26 \text{ kJ mol}^{-1}$$

Comparing ΔE_{planar} with $\Delta E_{stacked}$, it is clear that, while the formation of the planar dimer in the matrix is energetically neutral, the formation of the stacked dimer is unfavorable. This may explain why only the planar dimer is present in the argon matrix.

4.4. Accuracy of the Calculated Interaction Energies of the Quinone Dimers. In this work the interaction energies of the planar and stacked quinone dimers were calculated at the MP2/6-31+G* and MP2/6-31++G** levels of theory for the dimer geometries optimized at the MP2/6-31+G* level. In addition, the BSSE and ZPVE corrections were accounted for. There are two main reasons which can limit the accuracy of the calculated interection energies and their effect should be examined. These reasons are the incompleteness of the basis set used in the calculations, and neglecting the higher-order correlation energy contributions. The size of the dimer studied has precluded the use of more extended basis sets and a more sophisticated level of theory. In this situation, in order to estimate the accuracy of the present calculations, we need to refer to investigations of similar systems performed by others. The best example of a prototype system, which exemplifies the interaction of two aromatic molecules and has been calculated using an extended array of different quantum-mechanical methods and different basis sets,[26−29] is the benzene dimer. This system has also been extensively studied with various experimental methods.[30−35] In a detailed analysis performed by Hobza et al.,[26] the accuracy of different levels of the calculations has been examined for the parallel-displaced and T-shaped benzene dimers. It was demonstrated that due to the truncation of the basis set the real stabilization energy of the benzene dimers should be about 20% larger than the energy calculated at the MP2/DZ+2P level, although the relative stabilization of the two structures remains unchanged. Similar behavior can be expected in the calculations of the quinone dimers performed in the present work.

The effect of neglecting the contributions due to higher correlation effects may be estimated based on the results for the benzene−He complex.[36] The stabilization energies obtained at the MP4 and MP2 levels of theory for this complex with the 6-31+G* basis set are almost identical (64.2 and 63.7 cm^{-1}).[36] The investigations of the stacked aromatic dimers of pyrimidine, triazine, aminotriasine, and aminopyrimidine performed at the MP2 and CCSD(T) levels[37] also demonstrated that the MP2 calculations with a medium-size basis set augmented with diffuse orbitals produce interaction energies which are close to the values obtained with the more sophisticated CCSD(T) method. The present calculations should show a simmilar accuracy.

A comparison of the calculated and experimental dimer interaction energies is difficult since the experimental data for the stacked aromatic systems are very limited. The experimental stabilization enthalpy of 2.3 kcal mol^{-1} obtained for benzene by evaluating different bulk properties is in good agreement with the value of 2.4 kcal mol^{-1} calculated at the MP2/DZ+2P level.[26] Though limited, this data indicates that the level of the theory selected for the present study should provide results in a reasonably good agreement with the experiment.

5. Conclusions

The structures of weakly-bonded quinone dimers were studied by a combined experimental−theoretical approach. The matrix-

isolation IR spectroscopy was used to obtain spectra of the quinone monomer and the dimers isolated in Ar matrices. A set of quinone dimer bands was found in the fingerprint regions of the spectrum. The half-widths of the dimer bands were found to be similar to the half-widths of the bands of the monomer, suggesting that the quinone dimers have well-defined structures in the matrices. The observed shifts of the monomer bands due to the dimer formation do not exceed 10 cm^{-1}.

The experimentally-observed dimer bands were analyzed by comparing them with the harmonic IR frequencies calculated for the planar and stacked dimers at the DFT/B3LYP/6-31++G** level of theory. Almost perfect agreement between the frequency shifts observed in the IR spectrum and those predicted theoretically for the planar dimer was found. There was no match between any bands in the spectrum and the bands predicted in the calculations for the stacked dimer. We take this as a manifestation that the stacked dimer was absent from the matrix in the present experiment.

Acknowledgment. This work was supported in part by a NATO grant (CRG 973389), allowing the visit of Dr. S. Stepanian to the University of Arizona.

References and Notes

(1) McCarthy, W.; Plokhotnichenko, A. M.; Radchenko, E. D.; Smets, J.; Smith, D. M. A.; Stepanian, S. G.; Adamowicz, L. *J. Phys. Chem.* **1997**, *101A*, 7208.

(2) Plokhotnichenko, A. M.; Radchenko, E. D.; Stepanian, S. G.; Adamowicz, L. *Recent Res. Dev. Phys. Chem.* **1998**, *2*, 1087.

(3) McCarthy, W.; Smets, J.; Adamowicz, L.; Plokhotnichenko, A. M.; Radchenko, E. D.; Sheina, G. G.; Stepanian S. G. *Mol. Phys.* **1997**, *91*, 513.

(4) Saenger, W. *Principles of Nucleic Acid Structure*; Springer-Verlag: New York, 1984.

(5) Murphy, C. J.; Arkin, M. R.; Jenkins, Y.; Ghatlia, N. D.; Bossmann, S. H.; Turro, N. J.; Barton J. K. *Science* **1993**, *262*, 1025.

(6) Dandliker, P. J.; Holmlin, R. E.; Barton J. K. *Science* **1997**, *275*, 1465.

(7) Becker H. C.; Broo, A.; Norden B. *J. Phys. Chem.* **1997**, *101*, 8853.

(8) Florian, J.; Sponer, J.; Warshel, A. *J. Phys. Chem.* **1999**, *103*, 884.

(9) Hobza, P.; Sponer, J. *Chem. Phys. Lett.* **1998**, *288*, 7.

(10) Sponer, J.; Leszczynski, J.; Hobza, P. *J. Comput. Chem.* **1996**, *17*, 841.

(11) Hobza, P.; Sponer, P.; Polasek, M. *J. Am. Chem. Soc.* **1995**, *117*, 792.

(12) Sponer, J.; Leszczynski, J.; Hobza, P. *J. Phys. Chem.* **1996**, *100*, 5590.

(13) Sponer, J.; Leszczynski, J.; Hobza, P. *J. Biomol. Struct. Dyn.* **1996**, *13*, 695.

(14) Sponer, J.; Hobza, P. *Chem. Phys. Lett.* **1997**, *267*, 263.

(15) Plokhotnichenko, A. M.; Ivanov, A. Yu.; Radchenko, E. D.; Sheina, G. G.; Blagoi, Yu. P. *Low Temp. Phys.* **1993**, *19*, 732.

(16) Reva, I. D.; Plokhotnichenko, A. M.; Radchenko, E. D.; Sheina, G. G.; Blagoi, Yu. P. *Spectrochim. Acta* **1994**, *50A*, 1107.

(17) Radchenko, E. D.; Sheina, G. G.; Smorygo, N. A.; Blagoi, Yu. P. *J. Mol. Struct.* **1984**, *158*, 387.

(18) Binkley, J. S.; Pople, J. A. *Int. J. Quantum Chem.* **1975**, *9*, 229.

(19) Pople J. A.; Binkley, J. S.; Seeger, R. *Int. J. Quantum Chem., Quantum. Chem. Symp.* **1976**, *10*, 1.

(20) Boys, S. F.; Bernardi, F. *Mol. Phys.* **1970**, *19*, 553.

(21) Becke, A. D. *Phys. Rev. B* **1988**, *38*, 3098.

(22) Lee, C.; Yang, W.; Parr, R. G. *Phys. Rev. B* **1988**, *37*, 785.

(23) Vosko, S. H.; Wilk, L.; Nusair, M. *Can. J. Phys.* **1980**, *58*, 1200.

(24) Frisch, M. J.; Trucks, G. W.; Schlegel, H. B.; Gill, P. M. W.; Johnson, B. G.; Robb, M. A.; Cheeseman, J. R.; Keith, T.; Petersson, G. A.; Montgomery, J. A.; Raghavachari, K.; Al-Laham, M. A.; Zakrzewski, V, G.; Ortiz, J. V.; Foresman, J. B.; Cioslowski, J.; Stefanov, B. B.; Nanayakkara, A.; Challacombe, M.; Peng, C. Y.; Ayala, P. Y.; Chen, W.; Wong, M. W.; Andres, J. L.; Replogle, E. S.; Gomperts, R.; Martin, R. L.; Fox, D. J.; Binkley, J. S.; Defrees, D. J.; Baker, J.; Stewart, J. P.; Head-Gordon, M.; Gonzalez, C.; Pople, J. A. *Gaussian 94, Revision E.2*; Gaussian Inc.; Pittsburgh, PA, 1994.

(25) Verkin, B. I.; Prikhot'ko, A. F. *Cryocrystals* (in Russian); Naukova dumka: Kiev, Ukraine, 1983.

(26) Hobza, P.; Selzle, H. L.; Schlag, E. W. *J. Am. Chem. Soc.* **1994**, *116*, 3500.

(27) Hobza, P.; Selzle, H. L.; Schlag, E. W. *J. Phys. Chem.* **1993**, *97*, 3937.

(28) Rubio, M.; Torrens, F.; Sanchez-Marin, J. *J. Comput. Chem.* **1993**, *14*, 647.

(29) Hobza, P.; Selzle, H. L.; Schlag, E. W. *J. Chem. Phys.* **1990**, *93*, 5893.

(30) Scherzer, W.; Kratzschmar, O.; Selzle, H. L.; Schlag, E. W. *Z. Naturforsch.* **1992**, *47a*, 1248.

(31) Arunan, E.; Gutowsky, H. S. *J. Chem. Phys.* **1993**, *98*, 4294.

(32) Henson, B. F.; Hartland, G. V.; Venturo, V. A.; Felker, P. M. *J. Chem. Phys.* **1992**, *97*, 2189.

(33) Krause, H.; Ernstberger, B.; Neusser, H. *Chem. Phys. Lett.* **1991**, *184*, 411.

(34) Bornsen, K. O.; Selzle, H. L.; Schlag, E. W. *J. Chem. Phys.* **1986**, *85*, 1726.

(35) Fung, K. H.; Selzle, H. L.; Schlag, E. W. *J. Phys. Chem.* **1983**, *87*, 5113.

(36) Hobza, P.; Bludsky, O.; Selzle, H. L.; Schlag, E. W. *J. Chem. Phys.* **1992**, *97*, 335.

(37) Sponer, J.; Hobza, P. *Chem. Phys. Lett.* **1997**, *267*, 263.